

Complexation of Uranium(VI) with Aromatic Acids in Aqueous Solution: A Combined Computational and Experimental Study

Jonas Wiebke,[†] Anna Moritz,^{*†} Maja Glorius,^{*‡} Henry Moll,[‡] Gert Bernhard,[‡] and Michael Dolg[†]

Institut für Theoretische Chemie, Universität zu Köln, Greinstr. 4, D-50939 Köln, Germany, and Institut für Radiochemie, Forschungszentrum Dresden-Rossendorf e.V., P.O. Box 510119, D-01314 Dresden, Germany

Received November 2, 2007

The complexes of uranium(VI) with salicylhydroxamate, benzohydroxamate, and benzoate have been investigated in a combined computational and experimental study using density functional theory methods and extended X-ray absorption fine structure spectroscopy, respectively. The calculated molecular structures, relative stabilities, as well as excitation spectra from time-dependent density functional theory calculations are in good agreement with experimental data. Furthermore, these calculations allow the identification of the coordinating atoms in the uranium(VI)–salicylhydroxamate complex, i.e. salicylhydroxamate binds to the uranyl ion via the hydroxamic acid oxygen atoms and not via the phenolic oxygen and the nitrogen atom. Carefully addressing solvation effects has been found to be necessary to bring in line computational and experimental structures, as well as excitation spectra.

1. Introduction

Natural organic matter and microbes can influence the migration behavior of actinides, particularly of uranium, in the environment. For the assessment of risks connected, for example, with long-term nuclear waste disposal, knowledge of the binding modes of uranium under the various environmental conditions is important. Therefore, it is necessary to investigate the complex formation of uranium with selected bioligands, particularly with siderophores of the pyoverdinin type, which have a high potential to bind actinides.^{1–8} These natural ligands are secreted by ubiquitous aerobic soil bacteria of the genus

Pseudomonas to assimilate Fe(III) under iron-limiting conditions. *Pseudomonas* species have been found in former uranium mining areas in Saxony and Thuringia, Germany,⁹ and the secreted pyoverdins are known to mobilize uranium from shale mine tailings¹⁰ because of their unique uranium(VI)-binding properties.^{4,5,7} The preferred actinide binding functionalities of pyoverdins are the hydroxamic acid group at the peptide chain and the catechol group of the chromophore.^{3,11} In previous UV–vis¹² and time-resolved laser-induced fluorescence spectroscopy (TRLFS)¹³ studies of the complexation behavior of this hydroxamic acid group, salicylhydroxamic acid HOC₆H₄CONHOH (Hsha) and benzohydroxamic acid

* To whom correspondence should be addressed. E-mail: amoritz@uni-koeln.de (A.M.); m.glorius@fzd.de (M.G.). Phone: +49-(0)221-4706885 (A.M.); +49-(0)351-2602895 (M.G.). Fax: +49-(0)221-4706896 (A.M.); +49-(0)351-2603553 (M.G.).

[†] Institut für Theoretische Chemie.

[‡] Institut für Radiochemie.

- (1) Jarvis, N. V.; Hancock, R. D. *Inorg. Chim. Acta* **1991**, *182*, 229–232.
- (2) Brainard, J. R.; Strietelmeier, B. A.; Smith, P. H.; Langstonunkefer, P. J.; Barr, M. E.; Ryan, R. R. *Radiochim. Acta* **1992**, *58–9*, 357–363.
- (3) Albrecht-Gary, A.-M.; Blanc, S.; Rochel, N.; Ocaktan, A. Z.; Abdallah, M. A. *Inorg. Chem.* **1994**, *33*, 6391–6402.
- (4) Bouby, M.; Billard, I.; MacCordick, J. J. *Alloys Compds.* **1998**, *271*, 206–210.
- (5) Bouby, M.; Billard, I.; MacCordick, J. *Czech. J. Phys.* **1999**, *49*, 769–772.
- (6) Neu, M. P.; Matonic, J. H.; Ruggiero, C. E.; Scott, B. L. *Angew. Chem., Int. Ed.* **2000**, *39*, 1442–1444.

(7) Moll, H.; Glorius, M.; Bernhard, G.; Johnsson, A.; Pedersen, K.; Schäfer, M.; Budzikiewicz, H. *Geomicrobiol. J.* **2008**, in press.

(8) Moll, H.; Johnsson, A.; Schäfer, M.; Pedersen, K.; Budzikiewicz, H.; Bernhard, G. *BioMetals*. [Online early access] DOI: 10.1007/s10534-007-9111-x. Published online July 25, 2007. <http://www.springerlink.com/content/j488148478415886/>.

(9) Tzvetkova, T.; Flemming, K.; Selenska-Pobell, S. In *Annual Report 2001*; Fanghänel, T., Ed.; Institute of Radiochemistry, Forschungszentrum Rossendorf FZR-343: Dresden, Germany, 2001.

(10) Kalinowski, B. E.; Oskarsson, A.; Albinsson, Y.; Arlinger, J.; Ödegaard-Jensen, A.; Andlid, T.; Pedersen, K. *Geoderma* **2004**, *122*, 177–194.

(11) Budzikiewicz, H. *Fortschr. Chem. Org. Naturst.* **2004**, *87*, 83–205.

(12) Glorius, M.; Moll, H.; Bernhard, G. *Radiochim. Acta* **2007**, *95*, 151–157.

(13) Glorius, M.; Moll, H.; Geipel, G.; Bernhard, G. *J. Radioanal. Nucl. Chem.* **2008**, *277*, in press.

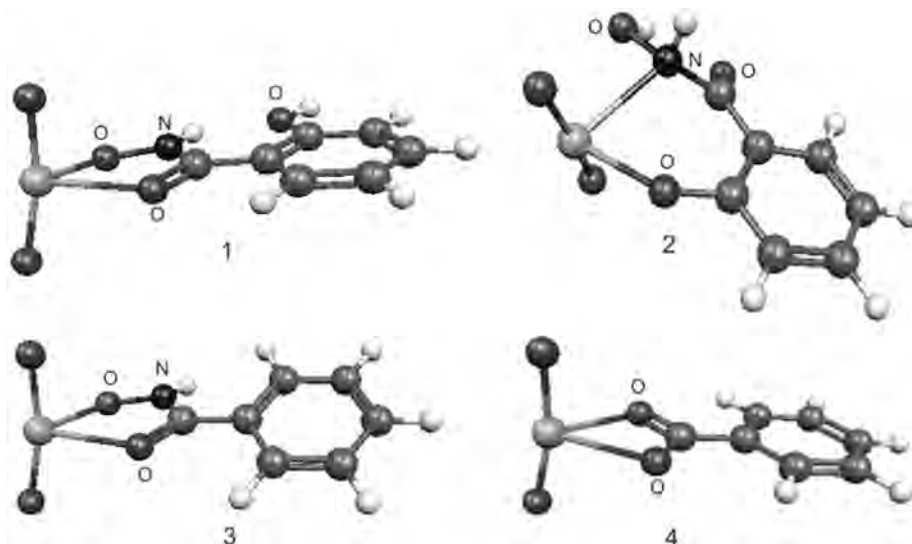


Figure 1. $[\text{UO}_2\text{L}]^+$ (L = sha, bha, ba) gas-phase molecular structures; 1, 2, 3, and 4 correspond to the [O,O]- and [N,O']-mode $[\text{UO}_2\text{sha}]^+$, to $[\text{UO}_2\text{bha}]^+$, and to $[\text{UO}_2\text{ba}]^+$, respectively.

$\text{C}_6\text{H}_5\text{CONHOH}$ (Hbha) were used as simple model ligands. As a comparison to the hydroxamic acids, benzoic acid $\text{C}_6\text{H}_5\text{COOH}$ (Hba) was also investigated. Both studies clearly show that the strength of the complex formation decreases from sha^- via bha^- to ba^- (stability constants $\log\beta([\text{UO}_2\text{sha}]^+) = 16.3$, $\log\beta([\text{UO}_2\text{bha}]^+) = 7.5$, $\log\beta([\text{UO}_2\text{ba}]^+) = 3.0$). Furthermore, the absorption and fluorescence properties of the uranium(VI) species formed with sha^- , bha^- , and ba^- were determined. If the uranyl ion UO_2^{2+} is coordinated by the hydroxamates sha^- or bha^- , a blue shift of the absorption maximum is observed, whereas coordination to the carboxylate ba^- results in a red shift of the absorption maximum with respect to the spectrum of the “free”, that is, water-coordinated, UO_2^{2+} .¹²

The structural data of actinide hydroxamate and benzoate species are scarce. The model ligands sha^- , bha^- , and ba^- were found as coordinating metal ions as bidentate ligands via the two hydroxamic^{14,15} and carboxylic oxygen atoms, respectively, with metal–oxygen distances of 1.88–1.98 Å in $\text{Cr(V)}-\text{sha}$ and $-\text{bha}$,¹⁶ 2.06 Å in $\text{Pt(II)}-\text{sha}$,¹⁷ 2.407 Å in $\text{U(VI)}-\text{ba}$,¹⁸ and 2.31 Å in $\text{Eu(III)}-\text{ba}$ ¹⁹ systems. Although sha^- is mainly discussed as coordinating metal ions via the two hydroxamic oxygen atoms ([O,O]-mode), there is at least one other reasonable coordination mode via the phenolic oxygen and the nitrogen atom ([N,O']-mode), compare Figure 1.

Although extended X-ray absorption fine structure (EXAFS) spectroscopy alone is often not sufficient to solve the structure of uranium(VI) species, particularly in the presence of mainly light backscattering atoms (C, N, O) in the near-order surrounding of the absorbing uranium atom, it has been shown^{20–28} that a combination of EXAFS spectroscopy and quantum chemical methods is a useful tool not only to investigate structures but also to estimate complex stabilities in solution, for example, of uranium(VI) hydroxides,^{27,28} fluorides,^{25,27} carbonates,²¹ and oxalates.^{25,26}

In this paper, we present a combined computational and experimental study using both EXAFS spectroscopy and density functional theory (DFT) calculations to determine precise molecular structures for the UO_2^{2+} complexes with the model ligands sha^- , bha^- , and ba^- and to clarify the coordination mode in the $[\text{UO}_2\text{sha}]^+$ complex. Furthermore, calculated relative stabilities and time-dependent DFT (TD-DFT)^{29–31} excitation spectra are compared to previous experimental stability constants^{12,13} and UV–vis spectra,¹²

- (14) Kurzak, B.; Kozłowski, H.; Farkas, E. *Coord. Chem. Rev.* **1992**, *114*, 169–200.
 (16) Gez, S.; Luxenhofer, R.; Levina, A.; Codd, R.; Lay, P. A. *Inorg. Chem.* **2005**, *44*, 2934–2943.
 (17) Hall, M. D.; Failes, T. W.; Hibbs, D. E.; Hambley, T. W. *Inorg. Chem.* **2002**, *41*, 1223–1228.
 (18) Vulpius, D. In *Zur Komplexbildung von Actiniden (U, Np) mit Hydroxybenzoesäuren*; Dresden University of Technology: Dresden, Germany, 2005.
 (19) Lam, A. W. H.; Wong, W. T.; Gao, S.; Wen, G. H.; Zhang, X. X. *Eur. J. Inorg. Chem.* **2003**, (1), 149–163.
 (15) Garcia, B.; Ibeas, S.; Leal, J. M.; Secco, F.; Venturini, M.; Senent, M. L.; Nino, A.; Munoz, C. *Inorg. Chem.* **2005**, *44*, 2908–2919.

- (20) Gutowski, K. E.; Cocalia, V. A.; Griffin, S. T.; Bridges, N. J.; Dixon, D. A.; Rogers, R. D. *J. Am. Chem. Soc.* **2007**, *129*, 526–536.
 (21) Ikeda, A.; Hennig, C.; Tsushima, S.; Takao, K.; Ikeda, Y.; Scheinost, A. C.; Bernhard, G. *Inorg. Chem.* **2007**, *46*, 4212–4219.
 (22) Gaillard, C.; Chaumont, A.; Billard, C.; Hennig, C.; Ouadi, A.; Wipff, G. *Inorg. Chem.* **2007**, *46*, 4815–4826.
 (23) Shamov, G. A.; Schreckenbach, G. *J. Phys. Chem. A* **2006**, *110*, 9486–9499.
 (24) Szabo, Z.; Toraiishi, T.; Vallet, V.; Grenthe, I. *Coord. Chem. Rev.* **2006**, *250*, 784–815.
 (25) Vallet, V.; Szabo, Z.; Grenthe, I. *Dalton Trans.* **2004**, (22), 3799–3807.
 (26) Vallet, V.; Moll, H.; Wahlgren, U.; Szabo, Z.; Grenthe, I. *Inorg. Chem.* **2003**, *42*, 1982–1993.
 (27) Vallet, V.; Wahlgren, U.; Schimmelpfennig, B.; Moll, H.; Szabo, Z.; Grenthe, I. *Inorg. Chem.* **2001**, *40*, 3516–3525.
 (28) Wahlgren, U.; Moll, H.; Grenthe, I.; Schimmelpfennig, B.; Maron, L.; Vallet, V.; Gropen, O. *J. Phys. Chem. A* **1999**, *103*, 8257–8264.
 (29) Bauernschmitt, R.; Ahlrichs, R. *Chem. Phys. Lett.* **1996**, *256*, 454–464.
 (30) Bauernschmitt, R.; Häser, M.; Treutler, O.; Ahlrichs, R. *Chem. Phys. Lett.* **1997**, *264*, 573–578.
 (31) Ingram, K.; Kaltsoyannis, N. In *Recent Advances in Actinide Sciences*; Alvarez, R.; Bryan, N. D.; May, I., Eds.; RCS Publishing: Cambridge, U.K., 2006.

respectively. Because all experiments are performed in aqueous solution, solvation effects are carefully addressed within the DFT calculations using both an explicit first hydration sphere for the UO_2^{2+} fragment and a continuum model.

2. Computational Details

The uranium(VI) complexes $[\text{UO}_2\text{L}]^+$ ($\text{L} = \text{sha}, \text{bha}, \text{ba}$) were completely geometry-optimized (symmetry C_1) at the DFT/B3LYP level^{32–37} using the TURBOMOLE, version 5.7 program system.³⁸ For $[\text{UO}_2\text{sha}]^+$, both the $[\text{O},\text{O}^-]$ - and the $[\text{N},\text{O}']$ -modes were considered. To ensure that the obtained structures are true energy minima on the potential energy surface (PES), numerical vibrational frequency analyses were performed. For uranium, the 5f-in-valence Wood–Boring pseudopotential (60 core electrons)³⁹ was used in combination with the (14s13p10d8f)/(10s9p5d4f) segmented contracted valence basis set.⁴⁰ The accuracy of this scalar-relativistic valence-only model for structures and binding energies, when used in combination with hybrid density functionals, was demonstrated, for example, by Batista et al.⁴¹ All other atoms were treated at the all-electron level using standard polarized triple- ζ (TZP) basis sets from the TURBOMOLE library. Except for the UO_2^{2+} oxygen atoms, all oxygen and nitrogen basis sets were augmented by one diffuse s-, p-, and d-function taken from the augmented correlation-consistent polarized valence double- ζ basis sets⁴² (exponents O $\alpha_s = 0.0790$, $\alpha_p = 0.0686$, $\alpha_d = 0.3320$; N $\alpha_s = 0.0612$, $\alpha_p = 0.0561$, $\alpha_d = 0.2300$). Because in TURBOMOLE, version 5.7,³⁸ exchange–correlation energies are numerically integrated on element specific grids and because no grid for uranium is implemented, all calculations were carried out employing the tungsten m5 grid by calculating the corresponding WO_2^{2+} systems and by setting the tungsten nuclear charge and mass to 92 and 238.03 u, respectively. Total energies were converged to 10^{-9} Hartree (scfconv = 9). In addition to the optimizations of $[\text{UO}_2\text{L}]^+$, calculations including solvation effects were also performed (see section 2.1).

The electronic excitations were treated within the adiabatic approximation of TD-DFT^{29,30} considering the 100 energetically lowest singlet excitations. For every calculated spectral

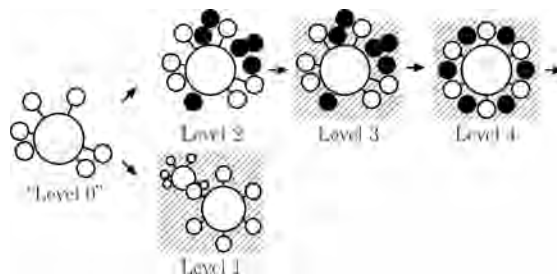


Figure 2. Different levels of addressing solvation effects. Note that there is no well-defined hierarchy among the levels 1 and 2.

line, one Gaussian function $a_0 \exp[-b(\lambda - \lambda_0)^2]$ was used to represent the contribution to the spectrum. Here a_0 is the oscillator strength, λ_0 is the wavelength, and $b = 0.005$ is a broadening parameter. The continuous spectrum in a given interval was obtained pointwise, as the sum over the 100 Gaussian functions, for each wavelength λ .

2.1. Modeling Solvation. Within a stationary quantum chemistry framework, one can address solvation effects on molecular and electronic structure by applying continuum models⁴³ or by modeling parts of or complete discrete solvation shells around the solute system of interest (levels 1 and 2, respectively, compare Figure 2). Moreover, one can combine both in a hybrid-type level 3 approach, modeling solute–solvent clusters for gas-phase conditions and correcting for long-range interactions by single-point energy calculations applying a continuum model. A level 4 approach would furthermore involve molecular structure relaxation within the continuum model potential.

Solvation effects on the $[\text{UO}_2\text{L}]^+$ and UO_2^{2+} systems have been modeled employing a hybrid-type level 3 approach. It has been shown in recent investigations of UO_2^{2+} hydration^{44–47} that this is a reliable strategy with inherent, but known shortcomings, which can be identified within a well-defined hierarchy of increasingly better approximations to aqueous solution conditions (compare Figure 2). Moreover, within a full level 4 approach, one encounters poor molecular structure convergence⁴⁴ or convergence to PES saddle points only,⁴⁵ which has been recently discussed to be an artifact because of the discretization of the solute cavity employed by the continuum models.⁴⁸

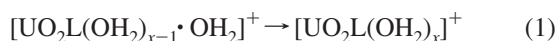
For level 3 single-point energy calculations, the conductor-like screening model (COSMO)⁴⁹ was used as implemented⁵⁰ in the TURBOMOLE, version 5.7 package.³⁸ The continuum permittivity was set to infinite. Solute cavities were con-

(32) Becke, A. D. *J. Chem. Phys.* **1993**, *98*, 5648–5652.
 (33) Lee, C. T.; Yang, W. T.; Parr, R. G. *Phys. Rev. B* **1988**, *37*, 785–789.
 (34) Becke, A. D. *Phys. Rev. A* **1988**, *38*, 3098–3100.
 (35) Vosko, S. H.; Wilk, L.; Nusair, M. *Can. J. Phys.* **1980**, *58*, 1200–1211.
 (36) Slater, J. C. *Phys. Rev.* **1951**, *81*, 385–390.
 (37) Dirac, P. A. M. *Proc. Camb. Phil. Soc.* **1930**, *26*, 376–395.
 (38) Ahlrichs, R.; Bär, M.; Baron, H. P.; Bauernschmitt, R.; Böcker, S.; Ehrig, M.; Eichkorn, K.; Elliott, S.; Furche, F.; Haase, F.; Häser, M.; Horn, H.; Huber, C.; Huniar, U.; Kölmel, C.; Kollwitz, M.; Ochsenfeld, C.; Öhm, H.; Schäfer, A.; Schneider, U.; Treutler, O.; Arnim, M.; Weigend, F.; Weis, P.; Weiss, H. *TURBOMOLE*, version 5.7; University of Karlsruhe: Karlsruhe, Germany, 2004.
 (39) Küchle, W.; Dolg, M.; Stoll, H.; Preuss, H. *J. Chem. Phys.* **1994**, *100*, 7535–7542.
 (40) Cao, X.; Dolg, M. *J. Mol. Struct.* **2004**, *673*, 203–209.
 (41) Batista, E. R.; Martin, R. L.; Hay, P. J.; Peralta, J. E.; Scuseria, G. E. *J. Chem. Phys.* **2004**, *121*, 2144–2150.
 (42) Kendall, R. A.; Dunning, T. H., Jr.; Harrison, R. J. *J. Chem. Phys.* **1992**, *96*, 6796–6806.

(43) Tomasi, J.; Mennucci, B.; Cammi, R. *Chem. Rev.* **2005**, *105*, 2999–3093.
 (44) Shamov, G. A.; Schreckenbach, G. *J. Phys. Chem. A* **2005**, *109*, 10961–10974.
 (45) Ingram, K. I. M.; Hüller, L. J. L.; Kaltsoyannis, N. *Dalton Trans.* **2006**, *20*, 2403–2414.
 (46) Moskaleva, L. V.; Krüger, S.; Spörl, A.; Rösch, N. *Inorg. Chem.* **2004**, *43*, 4080–4090.
 (47) Gutowski, K. E.; Dixon, D. A. *J. Phys. Chem. A* **2006**, *110*, 8840–8856.
 (48) Haller, J.; Kaltsoyannis, N. In *Recent Advances in Actinide Science*; Alvarez, R.; Bryan, N. D.; May, I., Eds.; RSC Publishing: Cambridge, U.K., 2006.
 (49) Klamt, A.; Schüürmann, G. *J. Chem. Soc., Perkin Trans.* **1993**, *2*, 799–805.
 (50) Schäfer, A.; Klamt, A.; Sattel, D.; Lohrenz, J. C. W.; Eckert, F. *Phys. Chem. Chem. Phys.* **2000**, *2*, 2187–2193.

structured using the COSMO default parameter set and the COSMO-RS atomic radii⁵¹ of 1.30, 2.00, 1.83, and 1.72 Å for H, C, N, and O, respectively, and 2.00 Å for U.⁴⁷ [UO₂sha(OH₂)₃]⁺ COSMO screening energies for U atomic radii varying within the 1.00–3.00 Å interval were found not to deviate from the 2.00 Å radius screening energy by more than 3 kJ mol⁻¹.

Because of computational feasibility and because the UO₂²⁺ fragment was expected to be the most strongly affected by solvation effects, a complete solvation shell was only modeled for the UO₂²⁺ fragment, that is, no discrete L⁻ solvation was considered. A realistic number *x'* of OH₂ ligands in the UO₂²⁺ equatorial plane was obtained from considering the rearrangements



with [UO₂L(OH₂)_{*x*-1}·OH₂]⁺ having *x* - 1 OH₂ ligands in the first and one OH₂ ligand in the second UO₂²⁺ solvation shell. Then, *x'* is the largest *x* for which the rearrangement 1 gives negative reaction energies. Within the level 3 approach, optimal molecular structures without and total energies within the COSMO potential have been calculated for the [UO₂sha(OH₂)_{*x*-1}·OH₂]⁺ (*x* = 3 and 4) and [UO₂sha(OH₂)_{*x*}]⁺ systems (*x* = 0, 1, 2, and 3). For [UO₂sha(OH₂)₄]⁺, no PES minimum structure was found, since during attempted structure optimizations the fourth OH₂ ligand moved out of the first UO₂²⁺ solvation shell to give [UO₂sha(OH₂)₃·OH₂]⁺ in all cases. For *x* = 3, [UO₂sha(OH₂)₃]⁺ is favored over [UO₂sha(OH₂)₂·OH₂]⁺ by 47 kJ mol⁻¹. Rigorously, from this one can only infer that *x'* = 3 is the minimum number of OH₂ ligands coordinated to the UO₂²⁺ fragment of [UO₂sha]⁺. However, *x'* = 3 fits best to experimental EXAFS coordination numbers. Moreover, for *x* = 0, 1, 2, and 3 the [UO₂sha(OH₂)_{*x*}]⁺ mean equatorial U–O_{eq} distances of 2.224, 2.330, 2.392, and 2.460 Å, respectively, approach the experimental EXAFS value of 2.41 Å as *x* increases. Although the *x* = 3 value is ~0.05 Å too large, this is known^{45,52–54} as a systematic level 3 overestimation of metal ion–OH₂ distances because of the neglect of molecular structure relaxation within the COSMO potential, which is the more severe the larger *x* is; this might also be caused by the DFT/B3LYP method, which has been shown to overestimate especially equatorial bond distances in PuO₂²⁺ complexes.⁵⁵ Therefore, [UO₂sha(OH₂)₃]⁺ is believed to be the most consistent structure model for the uranyl–sha system. Because of the great similarity of bha⁻ and ba⁻ with sha⁻ and because of the experimental EXAFS data, *x'* = 3 is assumed for the bha and ba systems, too. For [UO₂ba(OH₂)₃]⁺, however, no PES minimum, but only a first order PES saddle point was found in all cases; following that structure's ω = i 20.8 cm⁻¹ eigenmode did not lead to any PES minimum corresponding to a [UO₂ba(OH₂)₃]⁺

complex. Similar difficulties were stated for PuO₂²⁺ complexes⁵⁵ and attributed to the DFT/B3LYP method.

3. Experimental Section

3.1. Solutions and Reagents. A stock solution of 0.1 M uranyl perchlorate was prepared by dissolution of UO₃·0.77H₂O in 0.3 M HClO₄ and analyzed by inductively coupled plasma mass spectrometry (ICP-MS). Salicylhydroxamic acid (Sigma-Aldrich, Germany), benzohydroxamic acid, benzoic acid, and sodium perchlorate (Merck, Germany) were of analytical grade; all other reagents were provided by Merck, Germany.

The pH adjustments were made with HClO₄ and NaOH. The pH was measured (accuracy 0.05 units) with a glass electrode (BlueLine 16 pH, Schott–Geräte GmbH, Mainz, Germany) calibrated with standard buffer solutions and a WTW pH540GLP pH meter (WTW, Weinheim, Germany). For all experiments, the sodium concentration was kept constant at 0.1 M by addition of NaClO₄. EXAFS measurements were performed at fixed sha⁻, bha⁻, and ba⁻ concentrations of 8·10⁻³ M within a pH range of 2.5–4.0 and UO₂²⁺ concentrations of 1·10⁻³ and 5·10⁻³ M in the case of sha⁻ and bha⁻/ba⁻, respectively.

3.2. X-ray Absorption Spectroscopy Measurements. EXAFS measurements were carried out on the Rossendorf Beamline (ROBL) BM20 at the European Synchrotron Radiation Facility.⁵⁶ The samples were measured at room temperature using a water-cooled Si(111) double-crystal monochromator in channel cut mode (5–35 keV). The uranium L_{III}-edge spectra were collected either in fluorescence mode using a 13-element germanium solid-state detector or in transmission mode using argon-filled ionization chambers. For energy calibration of the spectra, the K-edge spectrum of an yttrium metal foil (first inflection point at 17 038 eV) was recorded simultaneously. The threshold energy *E*₀ of the uranium L_{III}-edge was defined as the root of the second derivative of the averaged spectra. The spectra were processed with the data analysis programs Sixpack/SamView (version 0.59)⁵⁷ and WinXAS (version 3.1).⁵⁸ Theoretical backscattering phase and amplitude functions were calculated from the FEFF8 code⁵⁹ for a 23 atom cluster using atomic positions of UO₂(CH₃COO)₂·2H₂O⁶⁰ and for a 42-atom cluster [UO₂NO₃(C₇H₄O₃)₂] using atomic positions of [UO₂NO₃(C₇H₄O₃)(C₇H₁₁N₂)₂].⁶¹ The multiple-scattering path U–O (axial, 4-legged path) was included in the model calculations. The amplitude reduction factor *S*₀² was held constant at 1.0 for all fits.

4. Results and Discussion

In the following the computational and experimental results for the molecular structures, the relative stabilities, and the excitation spectra of the uranium(VI) complexes formed with the model ligands sha⁻, bha⁻, and ba⁻ will be

(51) Klamt, A.; Jonas, V.; Bürger, T.; Lohrenz, J. C. W. *J. Phys. Chem. A* **1998**, *102*, 5074–5085.
 (52) Mochizuki, Y.; Tsushima, S. *Chem. Phys. Lett.* **2003**, *372*, 114–120.
 (53) Yang, T.; Bursten, B. E. *Inorg. Chem.* **2006**, *45*, 5291–5301.
 (54) Cao, Z.; Balasubramanian, K. *J. Chem. Phys.* **2005**, *123*, 114309–114309-12.

(55) Balasubramanian, K.; Chaudhuri, D. *Chem. Phys. Lett.* **2007**, in press.
 (56) Matz, W.; Schell, N.; Bernhard, G.; Prokert, F.; Reich, T.; Claussner, J.; Oehme, W.; Schlenk, R.; Diemel, S.; Funke, H.; Eichhorn, F.; Betzl, M.; Prohl, D.; Strauch, U.; Huttig, G.; Krug, H.; Neumann, W.; Brendler, V.; Reichel, P.; Denecke, M. A.; Nitsche, H. *J. Synchrotron Radiat.* **1999**, *6*, 1076–1085.
 (57) Webb, S. M. *Phys. Scr.* **2005**, *T115*, 1011–1014.
 (58) Ressler, T. *J. Synchrotron Radiat.* **1998**, *5*, 118–122.
 (59) Ankudinov, A. L.; Ravel, B.; Rehr, J. J.; Conradson, S. D. *Phys. Rev. B* **1998**, *58*, 7565–7576.
 (60) Howatson, J.; Grev, D. M.; Morosin, B. *J. Inorg. Nucl. Chem.* **1975**, *37*, 1933–1935.
 (61) Nassimbeni, L. R.; Rodgers, A. L.; Haigh, J. M. *Inorg. Chim. Acta* **1976**, *20*, 149–153.

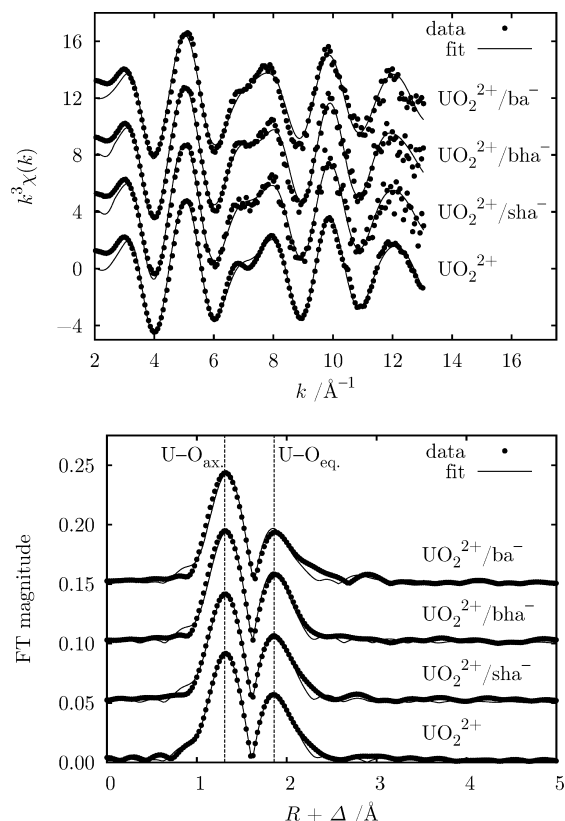


Figure 3. Uranium L_{III}-edge k^3 -weighted EXAFS spectra and corresponding Fourier transforms for the aqueous UO_2^{2+} and $\text{UO}_2\text{-L}$ ($\text{L} = \text{sha}, \text{bha}, \text{ba}$) systems including the best theoretical fits.

presented. In the case of the sha system, the preferred coordination mode, whether [O,O] or [N,O'], will be determined.

4.1. Molecular Structures. 4.1.1. EXAFS Structures.

Figure 3 shows the uranium L_{III}-edge k^3 -weighted EXAFS spectra and their corresponding Fourier transforms for the aqueous UO_2^{2+} and $\text{UO}_2\text{-L}$ ($\text{L} = \text{sha}, \text{bha}, \text{ba}$) systems. The small differences in the shape (amplitude and frequency) between the EXAFS oscillations of the “free”, that is, water-coordinated uranyl sample, and the ligand containing samples in the k -range 6–9 are attributed to the presence of uranyl complexes with the organic ligands. The structure parameters are summarized in Table 1. Generally, only small changes in the EXAFS structure parameters, indicating complex formation, have been observed. This might be connected with the comparably large fractions of 51%, 38%, and 28% “free” UO_2^{2+} in the sha, bha, and ba systems, respectively. Furthermore, for the two hydroxamate systems there are also 1:2 complexes $[\text{UO}_2\text{L}_2]$ present, which are in fact the dominant species. Thus, because of the overall similarity of the EXAFS structure parameters and the complicated composition of the EXAFS samples, it is very difficult to come to a definite interpretation of the data obtained.

In the two hydroxamate systems we observed mean U-O_{eq} bond lengths being by 0.01 Å shorter than in the “free” UO_2^{2+} . This decrease is in line with investigations on Pt(II)-sha^{17} and V(V)-bha^{62} complexes, where the mean

Table 1. U L_{III}-Edge EXAFS Results for the Aqueous UO_2^{2+} and $\text{UO}_2\text{-L}$ ($\text{L} = \text{sha}, \text{bha}, \text{ba}$) Systems^a

ligand	U(VI) speciation ^b	shell	N	R	σ^2	ΔE_0
sha ⁻	0.05 M UO_2^{2+} , pH 2.0 (100% UO_2^{2+})	U–O _{ax}	1.9	1.77	0.0016	10.5
		U–O _{eq}	5.0	2.42	0.0068	
		U–O _{ax}	2.2	1.77	0.0022	12.8
bha ⁻	0.001 M UO_2^{2+} , 0.008 M sha ⁻ , pH 2.5 (17% $[\text{UO}_2\text{sha}]^+$, 32% $[\text{UO}_2(\text{sha})_2]$, 51% UO_2^{2+})	U–O _{ax}	2 ^c	1.77	0.0014	13.0
		U–O _{eq}	4.6	2.41	0.0058	
		U–O _{ax}	2 ^c	1.78	0.0016	11.1
ba ⁻	0.005 M UO_2^{2+} , 0.008 M bha ⁻ , pH 3.5 (23% $[\text{UO}_2\text{bha}]^+$, 39% $[\text{UO}_2(\text{bha})_2]$, 38% UO_2^{2+})	U–O _{ax}	2 ^c	1.78	0.0016	11.1
		U–O _{eq}	4.7	2.43	0.0090	
		U–O _{ax}	2 ^c	1.78	0.0016	11.1
ba ⁻	0.005 M UO_2^{2+} , 0.008 M ba ⁻ , pH 4.0 (72% $[\text{UO}_2\text{ba}]^+$, 28% UO_2^{2+})	U–O _{ax}	2 ^c	1.78	0.0016	11.1
		U–O _{eq}	4.7	2.43	0.0090	
		U–O _{ax}	2 ^c	1.78	0.0016	11.1

^a Given are the coordination number N (error $\pm 15\%$), the bond length R (in Å; error ± 0.01 Å), the Debye–Waller factor σ^2 (in Å²), and the energy threshold ΔE_0 (in eV). ^b The U(VI) speciation was determined using the program SOLGASWATER.⁷⁴ ^c Parameter has been fixed during the fit.

equatorial metal–oxygen distances are also shortened because of the bidentate coordination via the hydroxamate oxygen atoms. In contrast to this, the mean U-O_{eq} distance in $[\text{UO}_2\text{ba}]^+$ is 0.01 Å larger than that of the “free” UO_2^{2+} , which is characteristic for bidentate coordination by ba^- .^{18,63,64} This data set’s explanatory power is clearly limited by the fact that the changes in the EXAFS structure parameters resulting from complex formation amount to the same order of magnitude as the experimental uncertainty does. Therefore, providing complementary molecular structure models from density functional calculations, as discussed in the following section, is believed to be of particular value.

4.1.2. Gas-Phase Structures. Figure 1 shows the calculated gas-phase molecular structures of $[\text{UO}_2\text{L}]^+$ ($\text{L} = \text{sha}, \text{bha}, \text{ba}$); for $[\text{UO}_2\text{sha}]^+$, both the [O,O]- and the [N,O']-modes are given. As one can see, the [N,O']-mode $[\text{UO}_2\text{sha}]^+$ has a very long U–N bond length and is clearly more distorted than the [O,O]-mode $[\text{UO}_2\text{sha}]^+$, which already suggests that the [N,O']-mode is less stable. In contrast to $[\text{UO}_2\text{bha}]^+$, the ligand of the [O,O]-mode $[\text{UO}_2\text{sha}]^+$ is in-plane. This is most likely the result of the phenolic hydroxyl group, which can interact with the NH group of the hydroxamic acid functionality and which is not present in the bha system. The ligand of $[\text{UO}_2\text{ba}]^+$ is again in-plane, so that this complex has C_s symmetry.

In Table 2, calculated gas-phase bond lengths and angles for UO_2^{2+} and $[\text{UO}_2\text{L}]^+$ ($\text{L} = \text{sha}, \text{bha}, \text{ba}$) are listed. Generally, the U-O_{ax} distances are found to increase if bare UO_2^{2+} is complexed. For UO_2^{2+} , where the EXAFS sample is pure (100% UO_2^{2+}), DFT underestimates the experimental U-O_{ax} distance by ~ 0.07 Å. For the complexes $[\text{UO}_2\text{L}]^+$, however, the DFT U-O_{ax} bond lengths are at most ~ 0.03 Å shorter than those given by EXAFS. These smaller deviations are most likely caused by an error cancelation, since the mean U-O_{ax} bond lengths, which are averaged

(63) Moll, H.; Geipel, G.; Reich, T.; Bernhard, G.; Fanghänel, T.; Grenthe, I. *Radiochim. Acta* **2003**, *91*, 11–20.

(64) Denecke, M. A.; Reich, T.; Pompe, S.; Bubner, M.; Heise, K. H.; Nitsche, H.; Allen, P. G.; Bucher, J. J.; Edelstein, N. M.; Shuh, D. K.; Czerwinski, K. R. *Radiochim. Acta* **1998**, *82*, 103–108.

(62) Liu, S.-X.; Gao, S. *Inorg. Chim. Acta* **1998**, *282*, 149–154.

Table 2. Bond Lengths, R (in Å), and Angles, \angle (in deg), as well as Binding Energies, E (in kJ mol⁻¹), for the Complexes [UO₂L]⁺ (L = sha, bha, ba) and the Bare Uranyl Ion UO₂²⁺ from DFT/B3LYP Gas-Phase Calculations^a

	[UO ₂ sha] ⁺				
	[O,O]	[N,O']	[UO ₂ bha] ⁺	[UO ₂ ba] ⁺	UO ₂ ²⁺
$R(U-O_{ax})$	1.757	1.760	1.755	1.749	1.698
	1.759	1.760	1.757	1.749	1.698
$R(U-O_{Carb})^b$	2.272		2.279	2.247	
$R(U-ON)$	2.175		2.178	2.247 ^c	
$R(U-O_{Ph})$		2.114			
$R(U-N)$		2.395			
$\angle O_{ax}-U-O_{ax}$	167.1	170.7	167.4	168.3	180.0
$\angle O_{Carb}-U-ON^b$	67.5		67.3	58.0 ^c	
$\angle N-U-O_{Ph}$		71.2			
E	1649	1610	1616	1510	

^a For [UO₂sha]⁺, the results for both the [O,O]- and the [N,O']-modes are given. ^b O_{Carb} is the oxygen atom of the carbonyl group. ^c In the case of the benzoate ligand ba⁻ the coordinating oxygen atom denoted as ON corresponds to the original hydroxyl group.

over all UO₂²⁺ species, appear too short because of the large “free” UO₂²⁺ fraction in the EXAFS samples. Furthermore, a reason for these underestimations is the neglect of solvation effects because additional water ligands in the equatorial plane increase the U–O_{ax} distances. Thus, the smaller deviations in the case of the complexes can also be explained by the fact that here only three instead of five equatorial water ligands are missing. In the case of the U–O_{eq} distances, one should not compare gas-phase DFT and EXAFS data because the gas-phase calculations consider UO₂²⁺ only as bi- and not as pentacoordinated. The comparison of the [N,O']-mode [UO₂sha]⁺ with the other complexes confirms the observation from Figure 1 that the U–N distance of 2.395 Å is quite long. The U–O_{eq} bond lengths in the hydroxamate systems [O,O]-mode [UO₂sha]⁺ and [UO₂bha]⁺ are nearly the same ($\Delta R_{max} = 0.007$ Å). The U–O_{eq} distances of the [UO₂ba]⁺ complex, however, deviate by up to 0.072 Å from those of the hydroxamate systems. A further change caused by the complex formation is that the linear O–U–O unit of UO₂²⁺ becomes slightly bent.

4.1.3. Solvated Structures. Table 3 shows the calculated structure parameters for the complexes [UO₂L(OH₂)₃]⁺ (L = sha, bha), as well as those for the solvated uranyl ion [UO₂(OH₂)₅]²⁺. Analogous to the gas-phase results, the U–O_{ax} distances in [UO₂(OH₂)₅]²⁺ increase if two water molecules are substituted by a bidentate hydroxamate ligand. But because of the consideration of the solvent effect, here the EXAFS values are only slightly under- and overestimated for [UO₂(OH₂)₅]²⁺ and [UO₂L(OH₂)₃]⁺, by approximately –0.02 Å and at most +0.01 Å, respectively. The comparison of the mean calculated bond lengths $\bar{R}(U-O_{eq})$ for the [O,O]- and [N,O']-mode [UO₂sha(OH₂)₃]⁺ with the EXAFS data indicates that sha⁻ is coordinated via the [O,O]-mode, since for this mode $\bar{R}(U-O_{eq})$ exceeds the experimental value only by ~0.05 Å as opposed to ~0.09 Å for the [N,O']-mode $\bar{R}(U-O_{eq})$. Furthermore, $\bar{R}(U-O_{eq})$ of the [N,O']-mode [UO₂sha(OH₂)₃]⁺ is larger than that of [UO₂(OH₂)₅]²⁺, which is the result of the very long U–N distance of 2.698 Å. For the [O,O]-mode sha and bha complex, however, the $R(U-O_{eq})$ values decrease by 0.036 and 0.035 Å compared to that of [UO₂(OH₂)₅]²⁺, respectively, which is qualitatively

Table 3. Bond Lengths, R (in Å), and Angles, \angle (in deg), for the Complexes [UO₂L(OH₂)₃]⁺ (L = sha, bha) and the Solvated Uranyl Ion [UO₂(OH₂)₅]²⁺ from DFT/B3LYP Calculations Including Solvation Effects Compared to Experimental (exptl) EXAFS Data^a

	[UO ₂ sha(OH ₂) ₃] ⁺			
	[O,O]	[N,O']	[UO ₂ bha(OH ₂) ₃] ⁺	[UO ₂ (OH ₂) ₅] ²⁺
$R(U-O_{ax})$	1.774	1.771	1.773	1.749
	1.776	1.775	1.775	1.749
$\bar{R}(U-O_{ax})$	1.775	1.773	1.774	1.749
$R_{exptl}(U-O_{ax})$	1.77	1.77	1.77	1.77
$R(U-O_{Carb})^b$	2.363		2.372	
$R(U-ON)$	2.284		2.292	
$R(U-O_{Ph})$		2.165		
$R(U-N)$		2.698		
$R(U-OH_2)$	2.537	2.516	2.538	2.495
	2.557	2.547	2.550	2.495
	2.560	2.574	2.552	2.496
				2.497
				2.497
$\bar{R}(U-O_{eq})$	2.460	2.500	2.461	2.496
$R_{exptl}(U-O_{eq})$	2.41	2.41	2.41	2.42
$\angle O_{ax}-U-O_{ax}$	169.1	174.4	169.4	179.8
$\angle O_{Carb}-U-ON^b$	65.8		65.9	
$\angle N-U-O_{Ph}$		64.7		

^a For [UO₂sha(OH₂)₃]⁺, the results for both the [O,O]- and the [N,O']-modes are given. ^b O_{Carb} is the oxygen atom of the carbonyl group.

in line with the EXAFS results; the fact that the EXAFS data give U–O_{eq} bond lengths decreasing only by 0.01 Å upon coordination is attributed to the large fraction of “free” UO₂²⁺ present in the EXAFS samples. $\bar{R}(U-O_{eq})$ of the [O,O]-mode sha and bha system differ only by 0.001 Å, which may explain why the EXAFS data show no difference. The overestimation of the experimental U–O_{eq} distances by 0.05, 0.05, and 0.08 Å for [O,O]-mode [UO₂sha(OH₂)₃]⁺, [UO₂bha(OH₂)₃]⁺, and [UO₂(OH₂)₅]²⁺, respectively, is connected with the shortcomings of our (level 3) solvation model, that is, the exclusive hydration of the UO₂²⁺ fragment and the neglect of bulk solvation effects and, possibly, of the DFT/B3LYP method. Here, the deviations for [UO₂L(OH₂)₃]⁺ are again smaller than that for [UO₂(OH₂)₅]²⁺ because of the large fraction of “free” UO₂²⁺ present in the EXAFS samples.

4.2. Relative Stabilities. The zero-point-corrected uranyl-ligand binding energies (compare Table 1) were obtained by $E = E(UO_2^{2+}) + E(L^-) - E([UO_2L]^+)$; the zero-point energies were scaled by 0.972.⁶⁵ Only gas-phase binding energies are given because explicit hydration was exclusively considered for the UO₂²⁺ fragment and not for ligands, resulting in energies that are too small, if calculated via $E = E([UO_2(OH_2)_5]^{2+}) + E(L^-) - E([UO_2L(OH_2)_3]^+)$. The comparison between the binding energies of the [O,O]- and [N,O']-mode [UO₂sha]⁺ shows that the latter complex is less stable by 39 kJ mol⁻¹. This confirms the conclusion based on the structure data that the sha⁻ ligand binds via the two hydroxamic acid oxygen atoms. Analogous to the experimental stability constants^{12,13} (compare section 1), the calculated binding energies demonstrate that the complex stabilities decrease from [O,O]-mode [UO₂sha]⁺ via [UO₂bha]⁺ to [UO₂ba]⁺ ($E = 1649, 1616, 1510$ kJ mol⁻¹ for sha, bha, and ba, respectively).

(65) Neugebauer, J.; Hess, B. A. *J. Chem. Phys.* **2003**, *118*, 7215–7225.

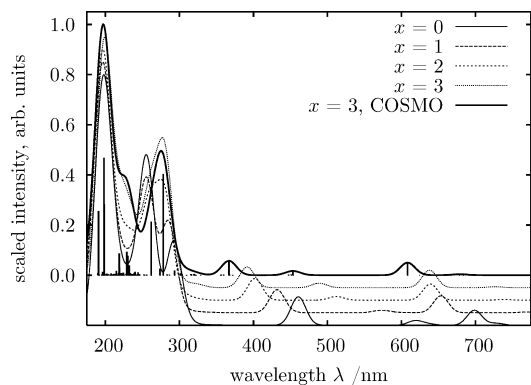


Figure 4. Calculated B3LYP TD-DFT excitation spectra for the $[\text{UO}_2\text{sha}(\text{OH}_2)_3]^+$ systems with $x = 0, 1, 2, 3$ and for $x = 3$ within the COSMO potential.

4.3. Electronic Spectra. The electronic spectrum of bare UO_2^{2+} has previously been discussed.⁶⁶ All transitions in the near-infrared and visible region are dipole-forbidden but may become allowed via interaction with equatorial ligands. Calculated bare UO_2^{2+} and $[\text{UO}_2\text{Cl}_4]^{2-}$ excitation energies were found to agree with experimental spectroscopic data for solid-state $\text{Cs}_2[\text{UO}_2\text{Cl}_4]$ within ~ 30 and 11 nm at MR-CISD (multireference configuration interaction including single and double substitutions)⁶⁷ and CASPT2 (complete active space second-order perturbation)⁶⁸ levels of theory, respectively; in contrast, however, it has recently been pointed out⁶⁹ that one cannot take for granted that excitation energies for the bare UO_2^{2+} calculated at TD-DFT levels of theory are always reliable.

Because of the C_1 symmetry of the systems studied here, only trivial (a_1) irreducible representations can be assigned to their electronic states. Because we are attempting a less formal discussion to support qualitative reasoning anyway, we instead focus on the systems (canonical Kohn–Sham) occupied and virtual molecular orbitals (MOs) which contribute to the electronic excitations calculated from the TD-DFT response functions. The MOs have been assigned to the UO_2^{2+} , L^- , and OH_2 subsystems of $[\text{UO}_2\text{L}(\text{OH}_2)_3]^+$ by their MO coefficients and Mulliken population analysis methods.

In Figure 4, the $[\text{O},\text{O}]$ -mode $[\text{UO}_2\text{sha}(\text{OH}_2)_3]^+$ excitation spectrum, calculated within the COSMO potential, is shown as a representative for both the sha and the corresponding bha system. Both systems' excitation spectra show three distinct groups of excitations which differ in wavelengths λ and relative intensities: large-intensity $\text{UO}_2^{2+} \leftarrow \text{OH}_2$ charge-transfer (CT) excitations with $\lambda \leq 200$ nm, $\text{L}^- \pi^* \leftarrow \pi$ excitations of intermediate intensities in the 200–300 nm range, and $\text{UO}_2^{2+} \leftarrow \text{L}^-$ CT excitations of low intensities in the 300–700 nm range. As shown in Figure 5, the experimental uranyl–sha and –bha systems' UV–vis spectra show one broad absorption band in the 350–450 nm range each,

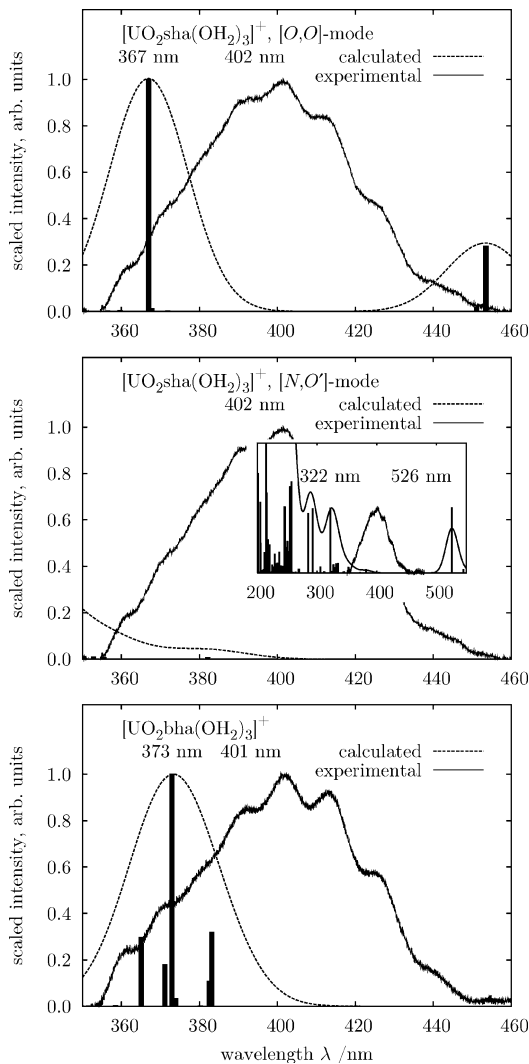


Figure 5. Calculated B3LYP TD-DFT spectra for the $[\text{O},\text{O}]$ - and $[\text{N},\text{O}']$ -mode $[\text{UO}_2\text{sha}(\text{OH}_2)_3]^+$ and the $[\text{UO}_2\text{bha}(\text{OH}_2)_3]^+$ systems and experimental¹² UV–vis spectra from aqueous solution. Calculated intensities have been scaled to have relative intensities of 1 for the 367, 322, and 373 nm excitations, respectively.

with absorption maxima at 402 and 401 nm, respectively.¹² The calculated absorption maxima of the $[\text{O},\text{O}]$ -mode $[\text{UO}_2\text{sha}(\text{OH}_2)_3]^+$ and $[\text{UO}_2\text{bha}(\text{OH}_2)_3]^+$ systems are at 367 and 373 nm, that is, blue-shifted by 35 and 28 nm or 0.29 and 0.23 eV, respectively, from the experimental absorption maxima. In the $[\text{O},\text{O}]$ -mode $[\text{UO}_2\text{sha}(\text{OH}_2)_3]^+$ excitation spectrum there is a second low-intensity excitation at 454 nm, that is, 52 nm or 0.35 eV from the experimental absorption maximum. All involve CT excitations from $\text{L}^- \pi$ MOs to U 5f atomic-orbital-like MOs. We assign the $[\text{O},\text{O}]$ -mode $[\text{UO}_2\text{sha}(\text{OH}_2)_3]^+$ 367 nm and the $[\text{UO}_2\text{bha}(\text{OH}_2)_3]^+$ 373 nm excitations to the corresponding experimental absorption maxima because, considering the calculated λ range of ~ 200 –700 nm, these match the latter within the expected systematic TD-DFT error and because experimental UV–vis spectra are dominated by large-intensity intramolecular ligand excitations for $\lambda < 350$ nm¹² as calculated. Moreover, when comparing to experimental data, one has to consider that the $\text{UO}_2^{2+} \leftarrow \text{L}^-$ complex formation is far from being quantitative, that is, that experimental

(66) Matsika, S.; Zhang, Z.; Brozell, S. R.; Blaudeau, J. P.; Wang, Q.; Pitzer, R. M. *J. Phys. Chem. A* **2001**, *105*, 3825–3828.

(67) Zhang, Z.; Pitzer, R. M. *J. Phys. Chem. A* **1999**, *103*, 6880–6886.

(68) Pierloot, K.; van Besien, E. *J. Chem. Phys.* **2005**, *123*, 204309–1–204309–10.

(69) Real, F.; Vallet, V.; Marian, C.; Wahlgren, U. *J. Chem. Phys.* **2007**, *127*, 214302–1–214302–11.

UV-vis spectra might be dominated by the “free”, though solvated, UO_2^{2+} ion's absorption bands centered at 414 nm.¹²

Compared to the [O,O]-mode, the calculated [N,O']-mode $[\text{UO}_2\text{sha}(\text{OH}_2)_3]^+$ excitation spectrum shows no suitable excitations in the 350–450 nm interval. There are $\text{L}^- \pi^* \leftarrow \pi$ and $\text{UO}_2^{2+} \leftarrow \text{L}^-$ CT excitations at 322 and 526 nm, being blue- and red-shifted by 80 and 124 nm or 0.77 and 0.73 eV, respectively, from the experimental sha-uranyl system's absorption maximum. Therefore, the [N,O']-mode may also be ruled out by comparison of its calculated spectrum with the experimental absorption spectrum.

We close this discussion by addressing some more general points: From the calculated excitation spectra of the series of [O,O]-mode $[\text{UO}_2\text{sha}(\text{OH}_2)_x]^+$ systems, as shown in Figure 4, one can see that accounting for solvation effects is important to bring calculated excitation spectra in line with experimental data. Neglecting solvation effects by setting $x = 0$ apparently gives a correct number and ordering of excitations, which are, however, significantly red-shifted with respect to both $x > 0$ and experimental data. Inclusion of discrete OH_2 ligands in the UO_2^{2+} equatorial plane improves the calculated excitation spectra as x increases. If $x = 3$, inclusion of the COSMO potential blue-shifts the $\text{UO}_2^{2+} \leftarrow \text{L}^-$ CT excitation from 391 to 367 nm, which is a large part of the 35 nm or 0.29 eV mismatch of the calculated excitation from the experimental absorption maximum. The fact that improving the solvation model with COSMO, that is, by going from a level 2 to a level 3 solvation model in Figure 2, causes a more pronounced mismatch of calculated and experimental absorption spectra is believed to point to our solvation model's shortcomings, that is, the neglect of discrete L^- subsystem solvation and the level 3 approximation of bulk solvation effects by a simple dielectric model. To address the question of exchange-correlation density functional dependency, the $[\text{UO}_2\text{sha}(\text{OH}_2)_3]^+$ excitation spectrum was recalculated using the gradient-corrected (GGA) PW91^{36,37,70} and BP86^{34–37,71} and the hybrid-type PBE0 functionals.^{36,37,70,72,73} GGA functionals were found to give excitation wavelengths up to 100 nm too large with respect to hybrid-type functionals, whereas the latter give a somewhat qualitatively consistent picture. However, using PBE0 TD-DFT, the $[\text{UO}_2\text{sha}(\text{OH}_2)_3]^+$ and $[\text{UO}_2\text{bha}(\text{OH}_2)_3]^+$ absorption maxima were calculated at 396 and 342 nm, whereas the experimental absorption maxima are at 402 and 401 nm, respectively. Thus, there appears to be no systematic functional dependency in quantitative terms.

5. Conclusion

The combined computational and experimental study of the uranyl complexes formed with the model ligands sha⁻,

bha⁻, and ba⁻ yields a consistent picture for the properties considered, that is, molecular structures, relative stabilities, and excitation spectra. The uranyl ion is found to be pentacoordinated by one bidentate ligand and three water molecules. The calculated mean U–O_{ax} and U–O_{eq} bond lengths of $[\text{UO}_2\text{L}(\text{OH}_2)_3]^+$ (L = sha, bha) and $[\text{UO}_2(\text{OH}_2)_5]^{2+}$ deviate from experimental EXAFS data by at most approximately –0.02 and +0.08 Å, respectively. The overestimation of the U–O_{eq} distances is caused by the known shortcomings of the applied (level 3) solvation model, that is, the exclusive hydration of the UO_2^{2+} fragment, the neglect of bulk solvation effects, and possibly, the DFT/B3LYP method. In the case of the relative stabilities, the experimental order is reflected by the calculated gas-phase binding energies, that is, the complex stabilities decrease from sha⁻ via bha⁻ to ba⁻. The calculated TD-DFT excitation and experimental UV-vis spectra of $[\text{UO}_2\text{L}(\text{OH}_2)_3]^+$ (L = sha, bha) are in good agreement, that is, the differences within the absorption maxima amount at most to 35 nm, corresponding to 0.29 eV. From molecular orbital considerations, the experimentally observed absorption bands are assigned to $\text{UO}_2^{2+} \leftarrow \text{L}^-$ charge transfer transitions. Because, in the case of $[\text{UO}_2\text{ba}(\text{OH}_2)_3]^+$, no DFT minimum structure could be obtained, for this complex the solvated molecular structure, as well as the excitation spectrum, are missing.

All considered properties demonstrate that the sha⁻ ligand binds via the two hydroxamic acid oxygen atoms. In the case of the [O,O]-mode, the agreement between experimental EXAFS and calculated mean U–O_{eq} bond lengths is clearly better ($\Delta R = 0.05$ and 0.09 Å for [O,O]- and [N,O']-mode, respectively); the calculated gas-phase binding energy is higher by 39 kJ mol^{-1} , and the deviation of the calculated from the experimental absorption maximum is about two times smaller than that for the [N,O']-mode ($\Delta\lambda = 35$ and 80 nm for [O,O]- and [N,O']-mode, respectively).

Acknowledgment. The financial support of the Deutsche Forschungsgemeinschaft (DFG) to J.W. and A.M. is gratefully acknowledged. The experimental work was funded by the BMWi under contract number 02E9985. EXAFS measurements were done at BM20 (ROBL) at the ESRF. We thank A. Rossberg, H. Funke, C. Hennig, and A. Scheinost for their help and support during the XAS experiments at ROBL. Furthermore, we wish to thank ACTINET, particularly J.-P. Flament, N. Kaltsoyannis, B. Schimmelpfennig, and V. Vallet, for providing an inspiring and encouraging atmosphere at the ACTINET ThUL School 2006 in Lille, where the current joint research project was initiated.

Supporting Information Available: Listings of input and DFT-optimized coordinates, as well as of obtained absolute energies. This material is available free of charge via the Internet at <http://pubs.acs.org>.

IC702162R

(70) Perdew, J. P.; Wang, Y. *Phys. Rev. B* **1992**, *45*, 13244–13249.

(71) Perdew, J. P. *Phys. Rev. B* **1986**, *33*, 8822–8824.

(72) Perdew, J. P.; Ernzerhof, K. B. M. *Phys. Rev. Lett.* **1996**, *77*, 3865–3868.

(73) Perdew, J. P.; Ernzerhof, M.; Burke, K. *J. Chem. Phys.* **1996**, *105*, 9982–9985.

(74) Puigdomenech, I. *Input, Sed, and Predom: Computer Programs Drawing Equilibrium Diagrams*; TRITA-OKK-3010; RIT: Stockholm, Sweden, 1983.